ELSEVIER

Contents lists available at ScienceDirect

Additive Manufacturing Letters

journal homepage: www.elsevier.com/locate/addlet



Short Communication

Application of micro-computed tomography for authentication of 3D printed composite parts



Gary Mac^a, Meenakshi Mandal^b, Aryan Rastogi^c, Gaffar Gailani^d, Hammond Pearce^{a,*}, Nikhil Gupta^a

- ^a Department of Mechanical and Aerospace Engineering, NYU Tandon College of Engineering, Brooklyn, NY, USA
- ^b Department of Electrical Engineering, Indian Institute of Technology Kanpur, Kanpur, Uttar Pradesh, India
- ^c Department of Electrical Engineering, Indian Institute of Technology Indore, Indore, Madhya Pradesh, India
- d Department of Mechanical Engineering Technology, New York City College of Technology, City University of New York, Brooklyn, NY, USA

ARTICLE INFO

ABSTRACT

Keywords:
Additive manufacturing
Fiber-reinforced polymers
Micro-computed tomography
Part authentication

Additive Manufacturing (AM) can apply unique customized printing patterns for each layer, which govern the microstructural features in a fiber-reinforced composite part. Non-destructive evaluation methods are used extensively to understand the defects and the microstructure of 3D printed composite parts. Considerable intellectual property is involved in designing and manufacturing composite parts, which needs to be protected using innovative methods. One of the concerns in this area is counterfeit parts made on high quality 3D printers, which need to be identified. This study aims to investigate and provide a part-authentication methodology for 3D printed composite parts by using the micro-computed tomography (µCT) scans of discontinuous fiber-reinforced polymer composite (FRPC) parts. The microstructure of FRPC contains fibers, matrix and porosity that are unique to the specimen and is a result of the printing parameters. Specimen A is printed with an infill direction of 90° and wall count of 3 and specimen B has the same infill direction but does not contain a wall boundary. A comparison between the different μ CT datasets of the specimens can identify the distinguishing features of the 3D printed composite part. The correlation developed across different µCT datasets from extracted features and the metrics formulated can be used to quantitatively differentiate the composite specimens. Frequency domain analysis shows the most promising results by correctly identifying 3 out of the 6 datasets belonging to the same AM. A part identification and authentication method for AM composites will be useful for identifying genuine or counterfeit parts and protect intellectual property.

1. Introduction

Additive Manufacturing (AM), also known as 3D printing, is a promising technology that offers unparalleled benefits over the traditional manufacturing methods such as casting or machining [1]. The inherent advantages of AM in developing complex geometrical structures with limited tooling and ensuring faster lead times [2] has led to its adoption in several industries such as automotive, aerospace, defense and biotechnology. AM involves developing the design in a digital format and transferred to a 3D printer that deposits the structural material layer-by-layer to form the volumetric parts. The transition from digital design to the manufactured part often results in discrepancies in the printed features of AM parts [3]. AM is described as a cyber-physical system [4], which offers a high degree of flexibility in customizing the overall supply chain [5]. A cyber-physical system has its own unique potential vulnerabilities that can compromise the quality of AM compo-

nents [6]. Research that studies material characteristics at a microstructural level of an AM part helps with defect identification and authentication of the part [7].

A number of studies have focused in the area of novel materials for the use in AM processes. Fiber-reinforced polymer composite (FRPC) parts are also manufactured by 3D printing [8]. FRPCs are develop to form lightweight and high performance parts by tailoring the filament size, placement, and patterns. Their mechanical properties and economic viability, along with the low production cycle time allow them to substitute metals like iron and aluminum in selective applications [8]. FRPCs are extensively used in the mass production of beams, rails, and front-end support systems in the automobile, aircraft, and construction industries, due to their high strength-to-weight ratio [9].

Development of composite feed materials has allowed several AM methods to be used for the manufacturing of FRPC parts. Today, the major AM techniques involving composite materials used commercially

E-mail addresses: gm1247@nyu.edu (G. Mac), meenakshim21@iitk.ac.in (M. Mandal), ee190002007@iiti.ac.in (A. Rastogi), ggailani@citytech.cuny.edu (G. Gailani), hammond.pearce@nyu.edu (H. Pearce), ngupta@nyu.edu (N. Gupta).

^{*} Corresponding author.:.

include vat photopolymerization and material extrusion. Continuous and short fiber reinforced filaments are widely for the material extrusion type printers. The fracture mechanics of 3D printed continuous fiber composites of varying fiber content can be optimized in different engineering applications [10]. 3D printed composites show a optimal strength to weight ratio and the applications of 3D printed composites have increased. Further mechanical property optimization of composite can be achieved by customizing the polymer matrix material and raster angle of fibers [11]. AM excels in the fabrication of sandwich-structured composites [12] and experimental study has shown the durability of these composites under different loading and environmental conditions [13].

Micro-computed tomography (μ CT) scans offer an nondestructive evaluation (NDE) method of imaging manufactured parts with a high resolution, which allows for detection of microstructural features on a fiber-level scale [14]. This 3D imaging technique scans a series of 2D cross-sectional images using X rays, and then reconstructs the images slice-by-slice to form a 3D model detailing the internal structure of the FRPC specimen. Several factors including directions of fibers, porosity, infill directions and others remain unique to the reconstructed model. Insitu defect detection methods for AM parts provide a continuous closed-loop feedback to ensure printing process stability and repeatability [15]. While μ CT scans are now widely used to determine defects in materials, capabilities for uniquely identifying similar specimens are still limited. AM methods are capable of printing highly repeatable quality specimens, and so further development of image processing, machine learning and analysis techniques for interpreting the μ CT scan is desired [16].

This study thus presents several methods for uniquely identifying a 3D printed part in a group of identical parts based on differences in their μ CT scans. The inherent structural properties of FRPCs allow for distinct identification of the composite parts based on fiber arrangement and defects such as porosity that are captured by the μ CT scans [17]. Defects can also be intentionally added to a design to reduce the strength of the AM part [18] and detection systems may be used to determine these compromises [19]. Based on the analysis of these distinctive properties, conclusive metrics are proposed which are derived from computervision algorithms. These metrics can be utilized to effectively demarcate the parts which differ from the reference part, and hence provide a robust part verification method that can be integrated in the AM supply chain. To the best of the authors' knowledge, this is the first work which investigates the use of μ CT scans for part identity verification.

The remainder of the paper is structured as follows: Section 2 provides a background and related work. Section 3 lists the process followed for construction of the datasets used for testing the different analytical methods, which are describe in Section 4. The results are discussed in Section 5, followed by the concluding remarks in Section 6.

2. Background

X-ray μ CT is often used in the evaluation of the quality of 3D printed composites and there are many technical challenges involved in the process [20]. It is very difficult to develop correlations between different μ CT image datasets even when the μ CT scans show the same specimen. The specimen needs to be placed onto a stand with putty for the μ CT scanning bed. The placement of the specimen on the scanning bed dictates the reconstruction axis for the μ CT images and for a 3D printed part, this reconstruction axis is often not perfectly aligned with the printed layers of the specimen. This results in some μ CT images showing multiple printed layers of the specimen in the same reconstructed image. For multiple μ CT scans of the same specimen, it is difficult to create a comparison between the different μ CT image datasets because the features from different layers bleeds into one image and introduces variation in μ CT images.

Methodologies and computed algorithms to analyze multiple μ CT image datasets for very similar printed specimens have limitations in their capability to identify similarities. Many defects identified within

the μ CT scans are attributed to non-optimal build conditions, manufacturing issues, and post-processing procedures [21]. A comparison of defects from different μ CT datasets would require a precise method to isolate the defects from the images. Image binarization method requires a single threshold input which is not enough to capture every defect of different shape and size in a μ CT image. Image characteristics like noise, shadows, masking, gamma, etc. also need to be accounted for to successfully formulate a viable method of distinguishing various defects in FRPC parts [22]. Reconstruction artifacts such as noise, scatter, beam hardening, and ring artifacts can be additions in the μ CT images that further add to the differentiation between the μ CT datasets of similar specimens. Three unconventional approaches are tested on a collection of μ CT datasets of similar FRPC parts to determine the optimal technique for identifying the unique characteristics of the features in the μ CT scans.

Frequency domain analysis techniques can be used to analyze digital signals such as images [23,24], speech [25], etc. The information encoded in each image is expressed in terms of basis functions. This helps in applying several transformations and filters to the image efficiently. For this method, the concept of power spectral density (PSD) is employed [26] to demarcate the datasets. PSD is defined as the measure of a signal's power content for a given frequency and it forms a strong feature which can represent the properties of the μ CT scan images.

Other methods for analyzing μ CT scans include histogram analysis [27] and audio spectrum analysis [28]. In the former method, the μ CT scans are preprocessed via image enhancement techniques, which are then used to plot a histogram based on their tone distribution and frequency intensity. Next, standard analysis can be done on the plots to determine conclusive metrics to differentiate the scans belonging to different specimens. Similarly, audio spectrum analysis is an indirect method of analyzing the scans. In this method, the scan images are converted to audio domain and their corresponding spectrograms are analyzed via several properties inherent to them.

3. Dataset construction

The specimens used in this study are rectangular specimens of length, thickness, and width of 4 in., 0.25 in., and 0.5 in., respectively. The computer-aided design (CAD) model of the specimen is created in Solid-Works 2020 and exported to a stereolithography (STL) file format. The STL file is imported into Ultimaker Cura software to define the printing parameters of the specimens. The common printing parameters of all specimens include 100 percent infill density, printing temperature of 240 °C, build plate temperature of 90 °C, and a layer height of 0.25 mm. Cura outputs a g-code file, which contains all the processing parameters and the set of instructions for the 3D printer. The specimens are printed on a FlashForge fused filament fabrication 3D printer using glass fiberreinforced acrylonitrile butadiene styrene (ABS) filament of 1.75 mm diameter manufactured by 3DXTECH. There are a total of 4 printed specimens created from the original CAD model. The structure of the layers of the specimens is depicted in Fig. 2, and the details of the printing parameters of the specimens are as follows:

- Specimen A and B are identical, with a exterior shell wall of count 3 and an infill direction of 90 degrees with respect to the horizontal length-wise axis of the model.
- Specimen C is printed with no exterior shell wall boundary and an infill direction of 90 degrees with respect to the length-wise axis of the model.
- 3. Specimen D is printed with an exterior shell wall of count 3 and an infill direction of 0 degrees with respect to the length-wise axis of the model.

The 4 printed specimens had to be cut for the computed tomography scan. A diamond saw blade is used to cut a small piece of 0.5 inch from the center of each printed specimens. A SkyScan 1172 μ CT scanner is used to process each of the specimens and generate an image dataset

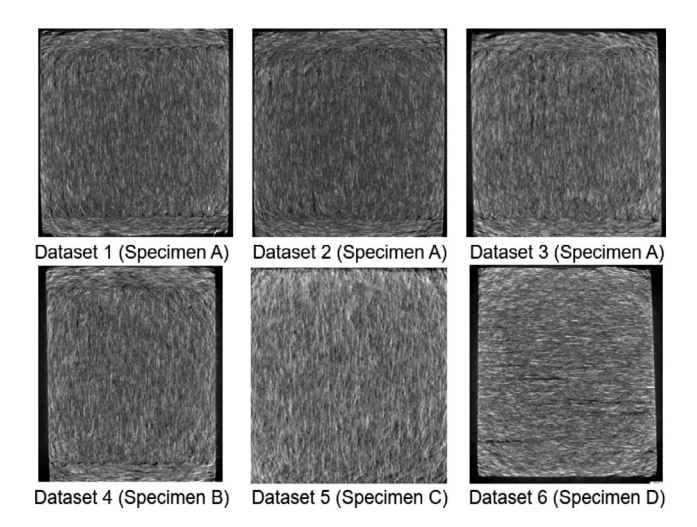


Fig. 1. Micro-computed tomography scans of four FRP specimens bifurcated under six datasets.

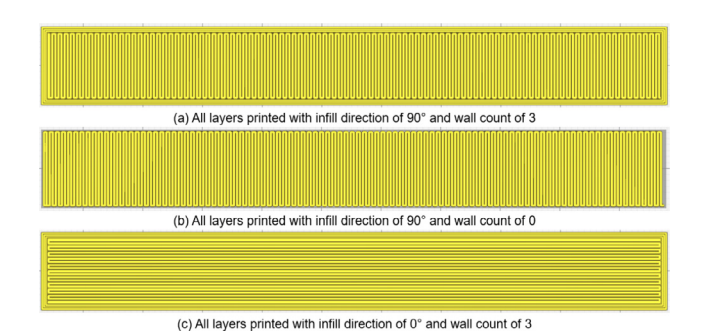


Fig. 2. Printing parameters used for (a) specimen A and B, (b) specimen C, and (c) specimen D.

for the microstructure of the printed specimens. The scan is conducted using camera pixel size of 9 source voltage of 40 kV, source current of 250 rotation step of 0.2° per scan, and 180° rotation. SkyScans NRecon reconstruction software is used to produce cross-section slices of the scanned specimen using a smoothing value of 2, ring artifact correction value of 18, and beam hardening correction value of 25 percent. There are 6 image datasets generated from the 4 printed specimens, which are shown in Fig. 1. Description of these datasets is mentioned below:

- 1. Dataset 1 is the result of the first μ CT of specimen A. The reconstruction software created 359 image slices.
- 2. Dataset 2 is also a μCT of specimen A. After specimen A was scanned and reconstructed, without removing the specimen from the scan bed, specimen A is scanned again to create a new image dataset of the specimen in the same position. Dataset 1 and 2 will capture identical features (such as fibres and porosity) from the specimen, but as reconstruction occurred separately, the dataset images will differ due to noise and manual selection results in a different total number of images. The reconstruction created 351 image slices of the specimen.
- 3. Dataset 3 is a third reconstruction of specimen A. After generating dataset 2, specimen A was removed from the scanning bed and flipped up-side down 180° before it is placed back into the μ CT machine. This dataset contains 372 images of the specimen. Dataset 3 contains very similar features as both dataset 1 and 2 but with the order of the images reversed.
- 4. Dataset 4 is a result of scanning specimen B. There are 376 images in this dataset. Specimen B has the same infill direction and wall boundary count as specimen A, but the microstructural fea-

- tures such as fiber and porosity contents from the μCT scans are different.
- 5. Dataset 5 is the image reconstruction of specimen C. There are 356 images in this µCT scan dataset. Specimen C is different from specimen A and B because it does not have the exterior shell wall boundary. Specimen C is expected to have a fair amount of similar attributes when compared with specimen A and B.
- 6. Dataset 6 is the image reconstruction of specimen D and there are 395 images. Specimen D is different from specimen A and B because it does not have the same infill printing direction. Specimen D is expected to have the most deviation in similarity when compared to the other 3 specimens.

A red-team blue-team approach was followed to avoid user bias in interpreting the similarity between each of the μCT datasets, where the blue team, consisting of the first author and latter three authors of the paper, are involved with printing of the specimens and generation of the μCT datasets. The red team, consisting of the second and third authors of the paper, are tasked with comparing the six μCT datasets and developing a metric to evaluate the similarity between each dataset with dataset 1. The red-team had no prior knowledge about the details of the datasets construction process and based their analysis solely on the features discovered in the images of the μCT datasets.

4. Methodology

The goal of this work is to identify efficient methods for distinctly identifying μ CT scans for the purposes of part authentication. The primary challenge is that differentiating features can only be observed at a very small scale, necessitating methods which can utilize the finegrained details within the μ CT scans to make decisive judgements on whether or not a scan belongs to a given specimen. Several potential methods which may be used to differentiate between the scans are presented and discussed in this section along with metrics for identification.

4.1. Preprocessing

Before the application of any of the following methods, the images from the original 6 datasets are preprocessed. This involves a cropping function to remove irrelevant objects and regions from the μ CT scan images. Also, overexposed and underexposed images are deleted in order to prevent detection of outliers which may lead to incorrect inferences. Both cropping and outlier removal are performed by importing the images in batch to ImageJ. Cropping is done manually by applying a square crop window to all the images to capture only the necessary details. Removal of images having the issue of abnormal color exposure is done by thresholding the images on the basis of the pixel values and excluding those images for which the area under the thresholded region deviated by a large margin from the rest of the images. The pixel threshold value in the above step is automatically determined by ImageJ, and does not required any manual intervention from the user. The number of μ CT scan images under each dataset after this preprocessing step are: Dataset 1 - 294, Dataset 2 - 298, Dataset 3 - 277, Dataset 4 - 276, Dataset 5 - 294, Dataset 6 - 266.

4.2. Fiber orientation detection

This method aims to find the ratio of the number of vertically aligned fibers to the number of horizontally aligned fibers in a μ CT scan, then use that fiber ratio (ϕ_f) for part differentiation. For each dataset, the preprocessed images files are imported in MATLAB, and gaussian filtering with a standard deviation of 2 is applied to denoise images and improve edge detection. Edge enhancement is applied via horizontal and vertical Sobel filters [29] to demarcate the regions of vertical and horizontal fibers within the image. Inbuilt functions *imgaussfilt* and *edge* are used for gaussian filtering and sobel edge detection respectively. As an

additional post-processing step, small artifacts identified by the filters having fewer than 100 pixels are removed by employing morphological operations (using *bwareopen* function of MATLAB). Thresholding is applied to the image to separately isolate the vertical and the horizontal identified fibers by setting the pixel values of the regions detected by Sobel filters to 1, and of the rest of the regions to 0. Lastly, the ϕ_f is calculated as:

$$\phi_f = \frac{A_{f_{90}}}{A_{f_0}} \tag{1}$$

where A_{f_0} is the area under the processed image belonging to the horizontal fibers and $A_{f_{90}}$ is the area for vertical fibers [30].

4.3. Histogram analysis

In histogram analysis, the preprocessed μ CT scans are loaded in MATLAB for image processing. Adaptive weiner filters are applied on datasets using inbuilt weiner2 function to remove Gaussian noise and reduce image variance for further morphological transformations. Salt and Pepper noises, present in negligible quantities (less than 1 percent), are ignored as a due matter of convenience. Thresholding of images by Otsu's method (using inbuilt graythresh function) is performed to segment image into object and background [31]. Prewitt filters are applied in images in both vertical and horizontal directions to detect and enhance edges (using edge function). Finally Principal Component Analysis (PCA) is applied on μ CT scans (using pca() function from Statistics Toolbox in MATLAB) to demarcate the regions of discontinuous frequency [32]. The average frequency of possible pixel values (8-bit integers) from 0 to 255 are tabulated by observing the intensity profile of datasets made using improfile function in MATLAB. The tabulated data is used to create histograms of respective datasets using inbuilt plot function in MATLAB.

Mean =
$$\frac{1}{n} \sum_{i=1}^{n} a_i = \frac{a_1 + a_2 + \dots + a_n}{n}$$
 (2)

The mean frequency for all pixel values are calculated for six datasets to find similarities and dissimilarities between them.

4.4. Audio spectrum analysis

The audio spectrum analysis on the μ CT datasets is analyzed in MATLAB. Linear filtering is applied on μ CT scans (using *imfilter* function) to remove both Gaussian noise and Impulse noise. Thresholding of images by Otsu's method (using inbuilt *graythresh* function) [31] is done to achieve image segmentation. Robert-Cross filters are applied in both vertical and horizontal directions to detect and enhance edges in images (using *edge* function). The images are then converted into binary matrices using in-built *imbinarize* function. Dark regions are labelled 1 while light regions are labelled 0. Lastly, these images are converted into 6-second long audio files in .wav format using the vOICe algorithm [33]. Regions denoted with 0 are assigned silence during the image-to audio conversion in the logarithmic scale. The amplitude of a specific region depends on the frequency of the pixels in that region. The mean amplitude (λ_{μ}) of waveforms across various datasets are calculated using the following equation:

$$\lambda_{\mu} = \frac{A_w}{\mathsf{T}} \tag{3}$$

where A_w represents the area under the waveform and T represents the total time taken in seconds. The λ_μ of the waveform averaged over all μ CT images of a dataset serves as a primitive metric to find similarities and dissimilarities across datasets.

4.5. Frequency domain analysis

The frequency domain analysis of the μ CT scans is done using MAT-LAB as follows: First, the μ CT scans are converted to frequency domain

Table 1Ouantitative metrics of different methods on the six *u*CT datasets.

Dataset	ϕ_f	Mean Frequency (Hz) (×10 ⁻³)	λ_{μ} (m) (×10 ⁻⁶)	MPSPSD (dB) (×10 ⁻⁴)
1	1.95	7468	-0.76	1.13
2	1.91	7428	-0.77	1.11
3	1.88	7475	-0.97	1.15
4	1.92	5987	-0.91	1.35
5	6.05	6110	-0.94	1.41
6	0.57	6587	-0.84	1.25

using the fast fourier transform (FFT) algorithm [34] by employing the inbuilt fft2 function and shifting the zero frequency component to the center of the frequency spectrum using fftshift function. Then, the magnitude of PSD is plotted against each frequency component of the image and the peak value of the PSD is found from the plot. Rescaling of the PSD magnitude by the total frequency points is done to ensure that the peak value calculated for images of different sizes was comparable. The net formulation of the above process can be expressed as:

$$PSD = 10\log_{10}(|\mathcal{F}(I)|^2)$$
 (4)

$$MPSPSD = max(PSD)/(n_{comp})$$
 (5)

where $\mathcal{F}(.)$ denotes the FFT function, I denotes the image and n_{comp} denotes the total frequency components of the image [35]. 'PSD' is a $1 \times n_{\text{comp}}$ dimensional array storing the PSD values of each frequency component in the array $\mathcal{F}(I)$ and 'MPSPSD' is the Maximum Peak of the Scaled PSD values calculated from 'PSD'. It is found that "MPSPSD" serves an effective metric for differentiating the μ CT images belonging to different datasets. The results are discussed comprehensively in Section 5.

5. Results and discussions

5.1. Results

The methodologies discussed in Section 4 are implemented on the datasets containing μ CT scans of four different specimens. At no given point during the analysis are the details about the dataset construction process (Section 3) made known to the red team, i.e., the team performing the analysis. Unless specified, the metrics proposed under the different methodologies are aggregated for all images corresponding to the same dataset. This aggregation is performed by simple averaging.

Table 1 presents the aggregated results obtained for each of the datasets using different methods. For the fiber orientation detection scheme (Section 4.2), in the " ϕ_f " column it can be seen that the specimens in datasets 5 and 6 differ significantly from the specimens in other datasets. This can be attributed to the high amounts of vertically aligned fibers and horizontally aligned fibers in dataset 5 and 6, respectively. It can be observed from the μ CT scans in Fig. 1 that most of the fibers in dataset 1–4 have a higher $A_{f_{90}}$ than A_{f_0} . Hence, the ϕ_f of dataset 5 is substantially higher than datasets 1-4 because it mostly contains vertically aligned fibers and does not have a outer wall boundary. The ϕ_f for dataset 6 is substantially lower because it contains a high amount of horizontally aligned fibers with a small amount of vertically aligned fibers at the edge due to the outer wall. However, this method is quite inconclusive to differentiate between specimens in datasets 1-4, since they possess a similar structure, and the difference in the number of vertical and horizontal fibers between each of them is not substantially high to warrant an observable difference in the ϕ_f . While the use of this method is limited to identifying major changes within the test specimen with respect to the reference specimen, however, it can be used in conjunction with other methods to provide an early-stage heuristic to identify potential mismatches between the test and the reference speci-

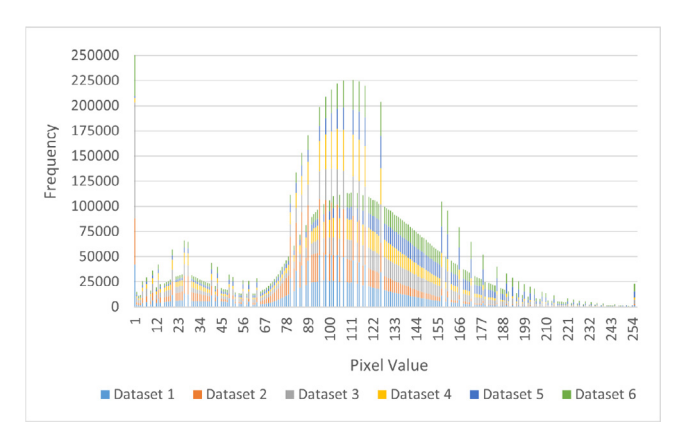


Fig. 3. Plot of histograms for all six datasets. The x and y axis of plot represent frequency intensity and pixel grayscale intensity value, respectively.

Histogram analysis is also performed on the scans, using the methodology discussed in Section 4.3. From Fig. 3, a frequency plot is shown for all the 6 datasets. It can be observed that datasets 4–6 show variation in the frequency at pixel values between 100 and 130. The histogram plot shows that there is a difference between datasets 4, 5, and 6 with the rest of the datasets. Furthermore, it can be inferred from Table 1 that datasets 1–3 are μ CT scans of the same FRPC specimen as their mean frequency show a low relative standard deviation of 0.34 percent. The mean frequency for dataset 4–6 shows that there is a clear distinction in the frequency of pixel values from dataset 1–3. Hence, it could be concluded that datasets 1–3 are μ CT scans of the same AM specimen while datasets 4–6 are identified as outliers.

An audio spectrum analysis is also performed to differentiate datasets based on μ CT scans in Fig. 1. Using Table 1, it can be inferred from the " λ_{μ} " column that the λ_{μ} of datasets 1 and 2 are significantly close, with a standard error of 5.0×10^{-7} . Furthermore, the nature of the waveforms in the logarithmic scale for datasets 1 and 2 are similar with a standard deviation of 7.07×10^{-7} . Hence, it could be concluded that datasets 1 and 2 are μ CT scans of the same AM specimen. However, the results obtained for datasets 3–6 remain inconclusive. Audio spectrum analysis effectively compares two specimens with similar tone distribution and waveform. Therefore, this method fails to differentiate between specimens in datasets 3–6. Audio spectrum analysis can be used as a metric that allows early-stage detection of possible matches of the test specimen with the reference specimen.

The frequency domain analysis was also performed on the datasets using the methodology as discussed in Section 4.5. From the "MPSPSD" results in Table 1, it can be seen that the values corresponding to the μCT scans in datasets 4-6 show a large deviation from those belonging to datasets 1-3. The MPSPSD values for the latter group of datasets are quite close to each other, with a standard deviation of 0.016. This observation points to the inference that the µCT scans in datasets 1-3 correspond to the same specimen. At the same time, the deviations in MPSPSD values for datasets 5 and 6 substantiates the inference obtained from the fiber ratios that specimens representative of datasets 5 and 6 indeed are different from the rest of the specimens, as well as from each other. In addition, this method is also able to similarly recognize dataset 4 as belonging to a distinct specimen. Thus, this method is able to accurately identify the correct distribution of the specimens in the six datasets used in the study. For a visualization of the MPSPSD values for each of the frequency points of a given μ CT scan, see Fig. 4.

5.2. Discussion

Almost all the methods discussed in this study show that they are able to accurately distinguish between the six datasets, i.e., identify datasets 1–3 belonging to the same FRPC specimen, and datasets 4–6 each be-

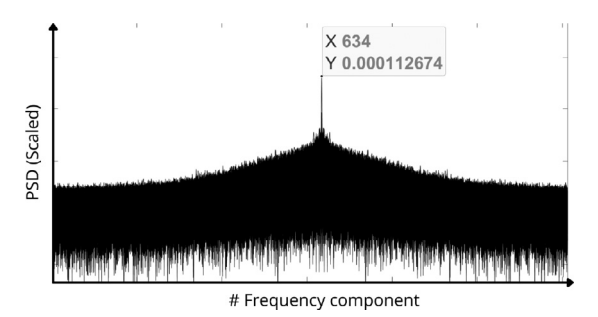


Fig. 4. Plot of scaled PSD values against different frequency components of a μ CT scan image for dataset 1. The Y value in the box denotes the MPSPSD value for the corresponding μ CT scan image.

longing to distinct specimens. Since dataset 3 essentially comprises of 180° flipped μ CT scans of the same specimen as of datasets 1 and 2, the methods are largely invariant to the orientation of the specimen during the scanning process. The fiber orientation method can be regarded as a preliminary method for distinctly authenticating the FRPC specimen, since it is only able to detect large scale changes in the structure of the specimen. However, given the relatively simple computation involved in the calculation of ϕ_f entailed by this method, it may be used in conjunction with the other methods to provide early stage warnings in case of a major mismatch between the test specimen and the target specimen.

The fiber orientation detection method provides conclusive data for printed specimens that have infill patterns for which the microstructure shows distinct fiber directions. For specimens printed using the same parameters like A and B, the fiber detection method cannot distinguish between the similar parts. This can be accounted for with the histogram analysis. From the mean frequency of all 6 datasets, histogram analysis is able to show that dataset 4 is different from dataset 1-3. The histogram analysis method is able to differentiate two specimens that were 3D printed with the same parameters. The analysis concluded that specimen C and D are also different from the rest of the dataset. The frequency domain analysis provided the same conclusion as the histogram analysis. The standard deviation from both methods for dataset 1-3 is a result of the inevitable imaging artifacts from the scanning process. These methods work because the number of fibers and porosity remains fixed for each individual 3D printed specimen. The μCT help to capture the minute differences in fiber and void content that differs even for specimens with the same printing parameters. The calculated mean frequency and MPSPSD values are sensitive to these differences and it shows that the datasets can be categorized based on their unique microstructural features.

The methods used in this study for analysis have (to the Authors' knowledge) been used for the first time in the context of evaluation of μ CT scan images in providing a metric to differentiate between different FRPC specimens. The results of all the methods are consistent with each other, which demonstrate their effectiveness towards authenticating the 3D printed composite parts. Another benefit of these methods is that they are highly scalable, not requiring high computational resources, thus enabling their deployment in practical scenarios to get near-real time monitoring of the AM supply chain.

6. Conclusions

This work focuses on determining the validity of different methods to extract features from a μ CT dataset of a AM produced composite specimen and develop a part authentication methodology. Although it is difficult to compare μ CT datasets of the same specimen due to reconstruction artifacts from the scanning process, the results from this work show that it is possible to identify μ CT datasets taken from the same specimen and thus differentiate it from other specimens. A method that can accurately label the μ CT dataset with its corresponding printed is

important for part authentication purposes in the AM supply chain. NDE studies have mostly focus on part quality assurance and gathering data to understand fracture mechanics of parts. This study has shown that the same data for quality assurance can be extended for part authentication in the manufacturing supply chain.

Data availability

Data will be made available on request.

CRediT authorship contribution statement

Gary Mac: Conceptualization, Methodology, Writing – original draft, Supervision. Meenakshi Mandal: Investigation, Writing – original draft. Aryan Rastogi: Investigation, Writing – original draft. Gaffar Gailani: Supervision, Writing – review & editing, Funding acquisition. Hammond Pearce: Writing – review & editing, Project administration. Nikhil Gupta: Conceptualization, Supervision, Funding acquisition.

Acknowledgments

This work was supported in part by National Science Foundation grants IRES OISE-1952479 and SaTC DGE-1931724.

References

- K.V. Wong, A. Hernandez, A review of additive manufacturing, Int. Sch. Res. Notices 2012 (2012), doi:10.5402/2012/208760.
- [2] S. Ford, M. Despeisse, Additive manufacturing and sustainability: an exploratory study of the advantages and challenges, J. Clean. Prod. 137 (2016) 1573–1587, doi:10.1016/j.jclepro.2016.04.150.
- [3] G. Mac, H. Pearce, R. Karri, N. Gupta, Uncertainty quantification in dimensions dataset of additive manufactured nist standard test artifact, Data Brief 38 (2021) 107286, doi:10.1016/j.dib.2021.107286.
- [4] M. Linares, N. Aswani, G. Mac, C. Jin, F. Chen, N. Gupta, R. Karri, Hack3d: crowd-sourcing the assessment of cybersecurity in digital manufacturing, Computer 54 (11) (2021) 58–67, doi:10.1109/MC.2021.3074192.
- [5] N. Gupta, A. Tiwari, S.T. Bukkapatnam, R. Karri, Additive manufacturing cyber-physical system: supply chain cybersecurity and risks, IEEE Access 8 (2020) 47322–47333, doi:10.1109/ACCESS.2020.2978815.
- [6] P. Mahesh, A. Tiwari, C. Jin, P.R. Kumar, A.L.N. Reddy, S.T.S. Bukkapatanam, N. Gupta, R. Karri, A survey of cybersecurity of digital manufacturing, Proc. IEEE 109 (4) (2021) 495–516, doi:10.1109/JPROC.2020.3032074.
- [7] S. Wang, H. Qu, S. Yu, S. Xia Zhang, Nondestructive investigation on close and open porosity of additively manufactured parts using an x-ray computed tomography, Mater. Today (2022), doi:10.1016/j.matpr.2022.08.559.
- [8] G.D. Goh, Y.L. Yap, S. Agarwala, W.Y. Yeong, Recent progress in additive manufacturing of fiber reinforced polymer composite, Adv. Mater. Technol. 4 (1) (2019) 1800271, doi:10.1002/admt.201800271.
- [9] M.A. Masuelli, Introduction of Fibre-reinforced Polymers Polymers and Composites: Concepts, Properties and Processes, Fiber Reinforced Polymers, IntechOpen, 2013, doi:10.5772/54629.
- [10] M.R. Khosravani, P. Frohn-Srensen, J. Reuter, B. Engel, T. Reinicke, Fracture studies of 3d-printed continuous glass fiber reinforced composites, Theor. Appl. Fract. Mech. 119 (2022) 103317, doi:10.1016/j.tafmec.2022.103317.
- [11] G. Sharma, A. Vuppuluri, K. Suresh, Essential work of fracture studies of 3d printed peek (poly-ether-ether-ketone) polymer, Eng. Fract. Mech. 271 (2022) 108656, doi:10.1016/j.engfracmech.2022.108656.
- [12] H. Bharath, D. Bonthu, S. Gururaja, P. Prabhakar, M. Doddamani, Flexural response of 3d printed sandwich composite, Compos. Struct. 263 (2021) 113732, doi:10.1016/j.compstruct.2021.113732.

- [13] M.R. Khosravani, A. Zolfagharian, M. Jennings, T. Reinicke, Structural performance of 3d-printed composites under various loads and environmental conditions, Polym. Test 91 (2020) 106770, doi:10.1016/j.polymertesting.2020.106770.
- [14] Q. Lu, N. Nguyen, A. Hum, T. Tran, C. Wong, Identification and evaluation of defects in selective laser melted 3161 stainless steel parts via in-situ monitoring and micro computed tomography, Addit. Manuf. 35 (2020) 101287, doi:10.1016/j.addma.2020.101287.
- [15] Y. AbouelNour, N. Gupta, In-situ monitoring of sub-surface and internal defects in additive manufacturing: a review, Mater. Design 222 (2022) 111063, doi:10.1016/j.matdes.2022.111063.
- [16] G. Chen, K. Yanamandra, N. Gupta, Artificial neural networks framework for detection of defects in 3d-printed fiber reinforcement composites, JOM 73 (2021), doi:10.1007/s11837-021-04708-9.
- [17] H. Srivastava, H. Pearce, G. Mac, N. Gupta, Determination of fiber content in 3-d printed composite parts using image analysis, IEEE Embed. Syst. Lett. 14 (3) (2022) 115–118, doi:10.1109/LES.2022.3140417.
- [18] H. Pearce, K. Yanamandra, N. Gupta, R. Karri, Flaw3d: a trojan-based cyber attack on the physical outcomes of additive manufacturing, IEEE/ASME Trans. Mechatron. (2022) 1–10, doi:10.1109/TMECH.2022.3179713.
- [19] C. Beckwith, H.S. Naicker, S. Mehta, V.R. Udupa, N.T. Nim, V. Gadre, H. Pearce, G. Mac, N. Gupta, Needle in a haystack: detecting subtle malicious edits to additive manufacturing g-code files, IEEE Embed. Syst. Lett. 14 (3) (2022) 111–114, doi:10.1109/LES.2021.3129108.
- [20] A. Palmquist, F.A. Shah, L. Emanuelsson, O. Omar, F. Suska, A technique for evaluating bone ingrowth into 3d printed, porous ti6al4v implants accurately using x-ray micro-computed tomography and histomorphometry, Micron 94 (2017) 1–8, doi:10.1016/j.micron.2016.11.009.
- [21] A. Wilbers, A. Biguri, J. Schillings, J. Loos, Application of iterative reconstruction algorithms to mitigate ct-artefacts when measuring fiber reinforced polymer materials, Polymer 177 (2019) 120–130, doi:10.1016/j.polymer.2019.06.004.
- [22] A. du Plessis, P. Sperling, A. Beerlink, L. Tshabalala, S. Hoosain, N. Mathe, S.G. le Roux, Standard method for microct-based additive manufacturing quality control 1: porosity analysis, MethodsX 5 (2018) 1102–1110, doi:10.1016/j.mex.2018.09.005.
- [23] B. Xu, Identifying fabric structures with fast fourier transform techniques, Text. Res. J. 66 (8) (1996) 496–506, doi:10.1177/004051759606600803.
- [24] W. Sun, L. Wang, E. Tutumluer, Image analysis technique for aggregate morphology analysis with two-dimensional fourier transform method, Transp. Res. Rec. 2267 (1) (2012) 3–13, doi:10.3141/2267-01.
- [25] C. Read, E.H. Buder, R.D. Kent, Speech analysis systems: an evaluation, J. Speech Lang. Hearing Res. 35 (2) (1992) 314–332, doi:10.1044/jshr.3502.314.
- [26] R.N. Youngworth, B.B. Gallagher, B.L. Stamper, An overview of power spectral density (psd) calculations, Opt. Manuf. Testing VI 5869 (2005) 206–216, doi:10.1117/12.618478.
- [27] M.G. Forero-Vargas, Fuzzy Thresholding and Histogram Analysis, in: Fuzzy Filters for Image Processing, Springer, 2003, pp. 129–152, doi:10.1007/978-3-540-36420-7_6.
- [28] A. Perović, Z. Đorđević, M. Paskota, A. Takači, A. Jovanović, Automatic recognition of features in spectrograms based on some image analysis methods, Acta Polytechnica Hungarica 10 (2) (2013) 153–172, doi:10.12700/aph.10.02.2013.2.11.
- [29] N. Kanopoulos, N. Vasanthavada, R.L. Baker, Design of an image edge detection filter using the sobel operator, IEEE J. Solid-State Circuits 23 (2) (1988) 358–367, doi:10.1109/4.996
- [30] M.E. Messiry, Theoretical analysis of natural fiber volume fraction of reinforced composites, Alexandria Eng. J. 52 (2013) 301–306, doi:10.1016/j.aej.2013.01.006.
- [31] N. Otsu, A threshold selection method from gray-level histograms, IEEE Trans. Syst. Man Cybern. 9 (1) (1979) 62–66, doi:10.1109/TSMC.1979.4310076.
- [32] A. Arab, J. Harbi, A. Abbas, Image compression using principle component analysis, Al-Mustansiriyah J. Sci. 29 (2018) 141, doi:10.23851/mjs.v29i2.256.
- [33] D. Brown, M. Proulx, Increased signal complexity improves the breadth of generalization in auditory perceptual learning, Neural Plast. 2013 (2013) 879047, doi:10.1155/2013/879047.
- [34] H.J. Nussbaumer, The Fast Fourier Transform, in: Fast Fourier Transform and Convolution Algorithms, Springer, 1981, pp. 80–111, doi:10.1007/978-3-642-81897-4_4.
- [35] S.L. Miller, D. Childers, 10 Power Spectral Density, in: Probability and Random Processes, Academic Press, 2004, pp. 369–411, doi:10.1016/B978-012172651-5/50010-5.